

Phase Shift Analysis of ${}^6\text{Li}$ Elastic Scattering on ${}^{12}\text{C}$ and ${}^{28}\text{Si}$ at $E_{lab} = 318$ MeV

Yong Joo KIM*

Department of Physics and Research Institute for Basic Sciences, Jeju National University, Jeju 63243, Korea

(Received 11 September 2018 : accepted 10 October 2018)

We present a three-parameter phase shift model whose form is the same as that of Coulomb-modified Glauber model obtained from Gaussian nuclear densities. This model is applied to the ${}^6\text{Li} + {}^{12}\text{C}$ and the ${}^6\text{Li} + {}^{28}\text{Si}$ elastic scatterings at $E_{lab} = 318$ MeV. The calculated differential cross sections provide quite a satisfactory account of the experimental data. The diffractive oscillatory structures observed at forward angles can be explained as being due to the strong interference between the near-side and the far-side scattering amplitudes. The optical potentials for two systems are predicted by using the method of inversion. The calculated inversion potentials are found to be in fairly good agreements with the results determined from the optical model analysis in the surface regions around the strong absorption radius. We also investigate the effects of parameters in the three-parameter phase shift model on the elastic scattering cross sections.

PACS numbers: 24.10.-i, 25.70.Bc

Keywords: Three-parameter phase shift model, Coulomb-modified Glauber model, McIntyre parametrized phase shift model, Phase shift analysis, ${}^6\text{Li}$ elastic scattering

I. INTRODUCTION

The differential cross section in the elastic scattering is an usually measured quantity in terms of scattering angle. The elastic angular distributions can be calculated from the scattering amplitude. A number of theoretical models [1,2] have been used to analyze the elastic scattering data. Nuclear phase shift is an important ingredient in the description of elastic differential cross section. Since the scattering matrix element related with nuclear phase shift is expressed in terms of a few parameters, the parametrized phase shift model (PPSM) have been conveniently adopted [3–7] to interpret the elastic scattering data at intermediate energies.

Meanwhile, the optical limit approximation (OLA) to the Glauber model [8], which neglects the correction terms in the expansion of the nucleus-nucleus phase shift function, has been used in the analysis of high energy elastic scattering data. If the nuclear density distribution is assumed to be Gaussian form, a nuclear phase

shift can be easily obtained as an analytic form [8,9]. The only parameter in nuclear phase shift is the ratio of real to imaginary part of the forward nucleon-nucleon (NN) amplitude because other input parameters are determined from nuclear densities and NN total cross section, respectively. The OLA to the conventional Glauber model was suitably modified [10] by taking into account the Coulomb distortion of the trajectory occurring in the nucleus-nucleus scattering. This type of OLA to the Glauber model is called as a “Coulomb-modified Glauber model (CMGM)”, and have been employed [5, 10] to study the elastic differential cross section at low and intermediate energies. In our earlier paper [11], we presented a nuclear-modified Glauber model using the classical perturbation of the Coulomb trajectory and it has been applied satisfactorily to the ${}^{16}\text{O} + {}^{28}\text{Si}$ and ${}^{16}\text{O} + {}^{40}\text{Ca}$ elastic scatterings at $E_{lab} = 1503$ MeV.

The elastic scatterings of 318 MeV ${}^6\text{Li}$ ions on ${}^{12}\text{C}$ and ${}^{28}\text{Si}$ target nuclei were measured [12]. Diffractive oscillations are observed at forward angles. The large angle data, which the cross sections down to a fraction of μb

*E-mail: yjkim@jejunu.ac.kr



were measured, are characterized by smooth exponential falloff pattern. Nadasen *et al.* [12] have used the optical and folding models to analyze this experimental data. This elastic scattering cross sections have also been studied [13] using the density-independent double folding optical potentials. Recently, an analysis of this elastic data has been made [14] within the framework of the first-order eikonal model.

Ahmad and Arafah [15] proposed a four-parameter phase shift model based on the Glauber model obtained from the modified harmonic oscillator target density, and shown that it provides an excellent fit to $\pi^\pm + {}^{12}\text{C}$ elastic scattering at 800 MeV/c. In this paper, we present a three-parameter phase shift model (TPPSM) deduced from the CMGM on the assumption of the Gaussian nucleus densities. The phase shift of TPPSM resembles the one of CMGM in shape and enable us to derive a closed expression for the optical potential by the method of inversion. It is interest to examine the usefulness of this model by applying it to the ${}^6\text{Li} + {}^{12}\text{C}$ and ${}^6\text{Li} + {}^{28}\text{Si}$ elastic scatterings at $E_{lab} = 318$ MeV. The calculated results will be compared with the ones obtained from CMGM and McIntyre PPSM, respectively. We will predict the optical potential using the method of inversion and its results also be compared with the Woods-Saxon optical potential determined from optical model analysis. Further, the effect of parameters in the TPPSM on the angular distributions will be investigated. In the following section, three-parameter phase shift model based on the CMGM is proposed. Sec. III provides the results and discussion, in which the TPPSM calculations for the elastic angular distribution and inversion potential will be performed and its results be compared with the ones of other models. Concluding remarks are given in Sec. IV.

II. THEORY

Ignoring the spin-orbit effect, the elastic scattering amplitude between two nuclei can be written in the form

$$f(\theta) = f_R(\theta) + \frac{1}{ik} \sum_{L=0}^{\infty} \left(L + \frac{1}{2}\right) \exp(2i\sigma_L) (S_L - 1) P_L(\cos\theta), \quad (1)$$

where $f_R(\theta)$ is the usual Rutherford scattering amplitude, σ_L is the Coulomb phase shift, $P_L(\cos\theta)$ is the Legendre polynomial, and S_L is the scattering matrix element. The S -matrix element, taking into account the Coulomb field, can be expressed in terms of nuclear phase shift $\delta_L(r_c)$ as

$$S_L = \exp[2i\delta_L(r_c)], \quad (2)$$

where r_c is the distance of closest approach given by

$$r_c = \frac{1}{k} (\eta + \sqrt{\eta^2 + L(L+1)}). \quad (3)$$

The elastic differential cross section is generally calculated from the scattering amplitude

$$\frac{d\sigma}{d\Omega} = |f(\theta)|^2. \quad (4)$$

Assuming nuclear density for both projectile (P) and target (T) as a Gaussian form

$$\rho_i(r) = \rho_i(0) \exp\left(-\frac{r^2}{a_i^2}\right), \quad i = P, T \quad (5)$$

the nuclear phase shift $\delta_L(r_c)$ in the Coulomb-modified Glauber model may be written [8,10,16] as

$$\delta_L(r_c) = \frac{A_P A_T \sigma_{NN}}{4\pi R^2} (\alpha_{NN} + i) \exp(-r_c^2/R^2), \quad (6)$$

where σ_{NN} is the NN total cross section, and α_{NN} is the ratio of the real to imaginary parts of the forward NN scattering amplitude. The σ_{NN} value is usually obtained from the relation [17]

$$\sigma_{NN} = \frac{N_P N_T \sigma_{nn} + Z_P Z_T \sigma_{pp} + N_P Z_T \sigma_{np} + N_T Z_P \sigma_{np}}{A_P A_T}, \quad (7)$$

where proton-proton cross section σ_{pp} (neutron-neutron cross section σ_{nn}) and neutron-proton cross section σ_{np} have been parametrized as a function of energy in Ref. [17]. At the same time, R is given by

$$R^2 = a_P^2 + a_T^2 + 2\beta_{NN}, \quad (8)$$

where β_{NN} is the slope parameter, and a_i is the Gaussian density parameter related with the root-mean-square radius R_{rms}^i as

$$a_i = \frac{R_{rms}^i}{\sqrt{1.5}}. \quad i = P, T \quad (9)$$

Table 1. Input parameters and χ^2/N values in the Coulomb-modified Glauber model (CMGM) and three-parameters phase shift model (TPPSM) for the ${}^6\text{Li} + {}^{12}\text{C}$ and ${}^6\text{Li} + {}^{28}\text{Si}$ elastic scatterings at $E_{lab} = 318$ MeV. 10% error bars are adopted to obtain χ^2/N values.

Target	CMGM					TPPSM			
	$a_P(fm)$	$a_T(fm)$	$\sigma_{NN}(mb)$	α_{NN}	χ^2/N	δ_{0R}	δ_{0I}	$c(fm^{-2})$	χ^2/N
${}^{12}\text{C}$	2.045	1.994	102.34	0.784	18.65	5.140	3.952	0.1036	3.05
${}^{28}\text{Si}$	2.045	2.528	102.34	0.856	19.75	8.530	5.893	0.0809	4.58

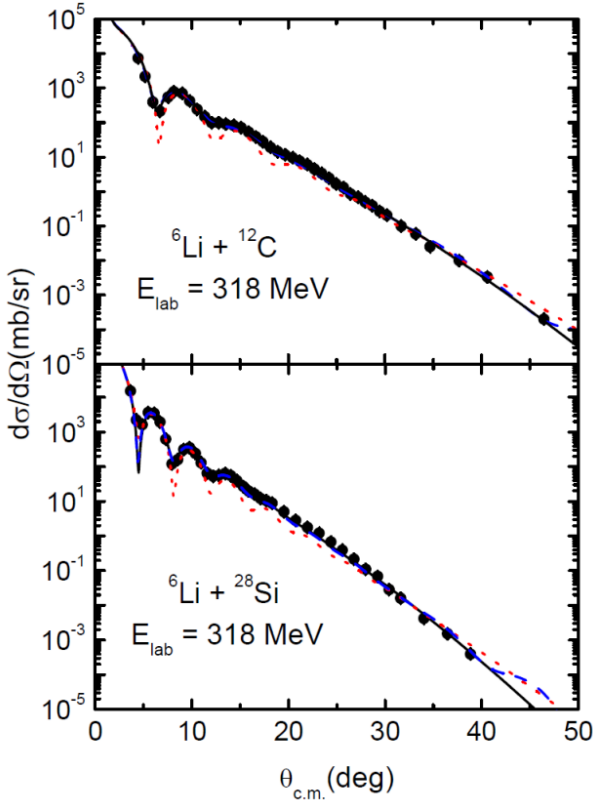


Fig. 1. (Color online) Elastic scattering angular distributions for the ${}^6\text{Li} + {}^{12}\text{C}$ and ${}^6\text{Li} + {}^{28}\text{Si}$ systems at $E_{lab} = 318$ MeV. The solid curves denote the results of three-parameter phase shift model. The dotted and dashed curves are the results using the Coulomb-modified Glauber and McIntyre parametrized phase shift models, respectively. The solid circles are experimental data taken from Ref. [12].

The phase shift Eq. (6) has been applied to the ${}^6\text{Li} + {}^{12}\text{C}$ and ${}^6\text{Li} + {}^{28}\text{Si}$ elastic scatterings at $E_{lab} = 318$ MeV. The only free parameter α_{NN} is determined from CMGM fit to the experimental data. In this calculation, the slope parameter β_{NN} is set equal to zero. Table 1 listed the density parameters (a_P and a_T) obtained from R_{rms}^i [17], NN total cross section (σ_{NN}) and the free input parameter α_{NN} , together with the values of χ^2/N . The calculated results of elastic differential cross

section are presented in Fig. 1 as dotted curves. We found that the nuclear phase shift of Eq. (6) does not provide satisfactory fits to the elastic scattering data. The qualities of fit in each system are poor especially around $10^\circ \sim 30^\circ$. These discrepancies are also reflected by the large χ^2/N -values as shown in Table 1. It seems that perhaps the phase shift Eq. (6) of CMGM is unsuitable for the description of 318 MeV ${}^6\text{Li}$ elastic scattering on ${}^{12}\text{C}$ and ${}^{28}\text{Si}$ targets.

This situation led us to parametrize the nuclear phase shift $\delta_L(r_c)$ in the following manner. Instead of nuclear phase shift of Eq. (6), we introduce a three-parameter phase shift model of the form:

$$\delta_L(r_c) = \delta_0 \exp[-cr_c^2], \quad (10)$$

where c is the real parameters and $\delta_0 (= \delta_{0R} + i\delta_{0I})$ is a complex parameters. This form of phase shift is the same as that of CMGM phase shift Eq. (6). From a comparison of the Eq. (6) with the expression Eq. (10), one can evaluate effective NN amplitude parameters (α_{NN} and σ_{NN}) and density parameters as follows:

$$\alpha_{NN} = \frac{\delta_{0R}}{\delta_{0I}}, \quad \sigma_{NN} = \frac{4\pi}{A_P A_T C} \delta_{0I}, \quad a_P^2 + a_T^2 = \frac{1}{c}. \quad (11)$$

Further, we can obtain a closed expression for the optical potential $U(r)$ by the inversion formula [10,18] :

$$U(r) = \frac{4E}{k\pi} \frac{1}{r} \frac{d}{dr} \int_r^\infty \frac{\delta(r_c)}{\sqrt{r_c^2 - r^2}} r_c dr_c. \quad (12)$$

Thus, the resulting expression for the optical potential can be written as

$$U(r) = V(r) + iW(r) = -\frac{4E\sqrt{c}}{k\sqrt{\pi}} \delta_0 \exp[-cr^2]. \quad (13)$$

Table 2. Input parameters and χ^2/N values in the McIntyre parametrized phase shift model for the ${}^6\text{Li} + {}^{12}\text{C}$ and ${}^6\text{Li} + {}^{28}\text{Si}$ elastic scatterings at $E_{lab} = 318$ MeV. 10% error bars are adopted to obtain χ^2/N values.

Target	L_g	Δ_g	L'_g	Δ'_g	μ	χ^2/N
${}^{12}\text{C}$	29.4012	6.1409	17.5241	5.8743	3.922	4.16
${}^{28}\text{Si}$	46.0574	7.1066	33.3364	6.5568	3.580	6.15

III. RESULTS AND DISCUSSION

A three-parameter phase shift model mentioned in previous section has been applied to the ${}^6\text{Li} + {}^{12}\text{C}$ and ${}^6\text{Li} + {}^{28}\text{Si}$ elastic scatterings at $E_{lab} = 318$ MeV. The calculations were carried out with χ^2/N -fit to the experimental data by treating δ_{0R} , δ_{0I} and c as adjustable parameters. The corresponding input parameter values are listed in Table 1, together with the χ^2/N -values. The calculated results of elastic differential cross sections are displayed in Fig. 1 as solid curves. The experimental data are taken from the work of Nadasen *et al.* [12]. The calculations have been found to reproduce well the elastic cross section data characterized by both the diffractive oscillatory structure (forward angles) and smooth exponential falloff pattern (large angles). It is seen that the overall fits to the experimental data are quite good. As Table 1 shows, reasonable χ^2/N -values are obtained for each scattering system.

Meanwhile, the phase shift based on McIntyre parametrization [3,4] contains five adjustable parameters and is expressed as

$$\delta(L) = \mu \left[1 + \exp\left(\frac{L - L'_g}{\Delta'_g}\right) \right] + i \frac{1}{2} \ln \left[1 + \exp\left(\frac{L_g - L}{\Delta_g}\right) \right]. \quad (14)$$

To investigate the usefulness of three-parameter phase shift model, we used this McIntyre parametrized phase shift model to calculate the angular distributions of 318 MeV ${}^6\text{Li}$ elastic scattering on ${}^{12}\text{C}$ and ${}^{28}\text{Si}$ target nuclei. The input parameters are given in Table 2, and the corresponding results are shown in Fig. 1 as dashed curves. As shown in this figure, the dashed curves seem to provide acceptable fits to the experimental data over the whole angular range. However, the solid curves gave somewhat more close to the experimental data than the dashed curves. In other words, though suggested phase shift involves three free parameters, the results (solid curves) obtained from Eq. (10) were found to do better

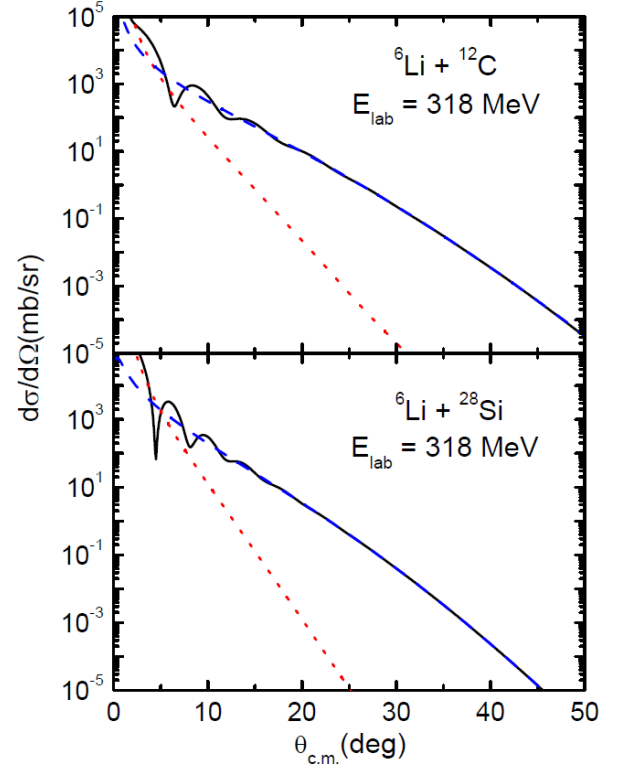


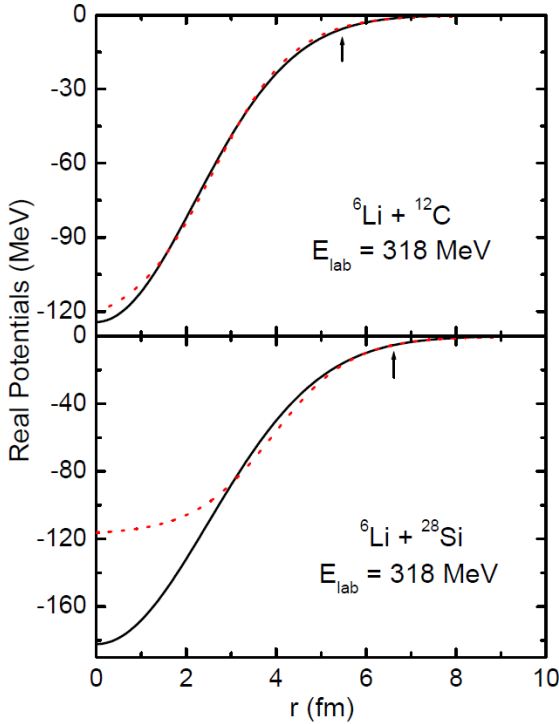
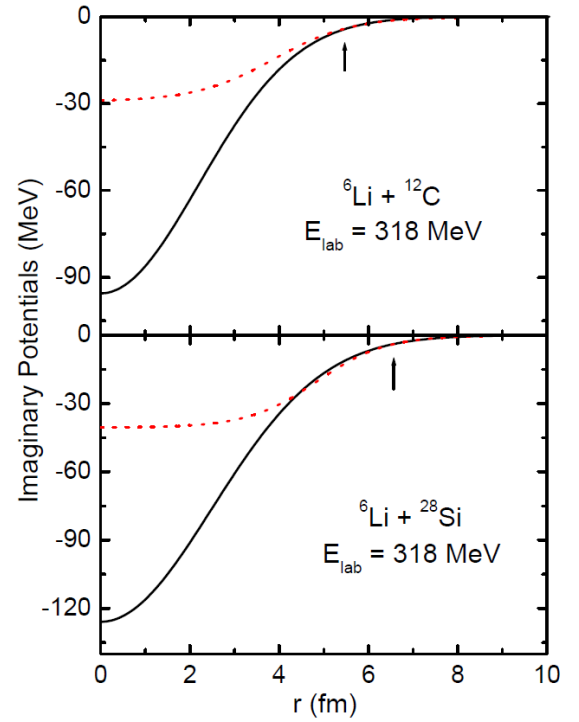
Fig. 2. (Color online) Differential cross sections (solid curves), near-side contributions (dotted curves), and far-side contributions (dashed curves) following the Fuller's formalism [19] using the three-parameter phase shift model for ${}^6\text{Li} + {}^{12}\text{C}$ and ${}^6\text{Li} + {}^{28}\text{Si}$ elastic scatterings at $E_{lab} = 318$ MeV.

in reproducing the experimental data than those (dashed curves) from phase shift Eq. (14) having five free parameters. As Table 1 and 2 show, the χ^2/N -values for each system are lower in the calculated results with Eq. (10) than the ones with Eq. (14). It may be said that three-parameter phase shift model is an alternative for describing the heavy-ion elastic scattering.

The structure of angular distributions for the ${}^6\text{Li} + {}^{12}\text{C}$ and ${}^6\text{Li} + {}^{28}\text{Si}$ elastic scatterings can be understood by the near-side and the far-side decompositions [19] of the scattering amplitude using the three-parameter phase shift model. Fig. 2 presents the results of the near-

Table 3. Analysis results of the Coulomb-modified Glauber (Cal. 1), three-parameter phase shift (Cal. 2) and McIntyre parametrized phase shift (Cal. 3) models for the ${}^6\text{Li} + {}^{12}\text{C}$ and ${}^6\text{Li} + {}^{28}\text{Si}$ elastic scatterings at $E_{\text{lab}} = 318$ MeV.

	$L_{1/2}$		$R_s(fm)$		$\sigma_{R_s}(mb)$		$\sigma_R(mb)$	
	${}^{12}\text{C}$	${}^{28}\text{Si}$	${}^{12}\text{C}$	${}^{28}\text{Si}$	${}^{12}\text{C}$	${}^{28}\text{Si}$	${}^{12}\text{C}$	${}^{28}\text{Si}$
Cal. 1	34.23	51.72	5.51	6.75	955	1433	988	1453
Cal. 2	34.11	50.54	5.49	6.60	948	1369	991	1403
Cal. 3	34.81	52.32	5.60	6.83	987	1465	1073	1520

Fig. 3. (Color online) Real parts of the optical potential for ${}^6\text{Li} + {}^{12}\text{C}$ and ${}^6\text{Li} + {}^{28}\text{Si}$ elastic scatterings at $E_{\text{lab}} = 318$ MeV. The solid curves denotes the potentials by the method of inversion, while the dotted curves are the potential determined by the optical model analysis [12]. The arrows indicate the position of the strong absorption radius.Fig. 4. (Color online) Same as Fig. 3, but for the imaginary parts of optical potential for ${}^6\text{Li} + {}^{12}\text{C}$ and ${}^6\text{Li} + {}^{28}\text{Si}$ elastic scatterings at $E_{\text{lab}} = 318$ MeV.

side (dotted curves) and far-side (dashed curves) contributions to the elastic scattering cross sections, along with the differential cross sections (solid curves). The diffractive oscillatory structures observed at forward angles can be interpreted as being due to the strong interference between the near-side and far-side components. As Fig. 2 shows, the magnitudes of the near-side and the far-side contributions are about the same at the crossing angles $\theta_{\text{cross}} = 4.1^\circ$ for ${}^6\text{Li} + {}^{12}\text{C}$ and $\theta_{\text{cross}} = 4.9^\circ$ for ${}^6\text{Li} + {}^{28}\text{Si}$. However, the far-side component becomes more dominant at angle regions greater than the crossing angles. Consequently, the far-side amplitude plays a key

role in determining the smooth exponential falloff behavior of large-angle cross section.

In Table 3, we presented the critical angular momenta $L_{1/2}$, strong absorption radii R_s and reaction cross sections σ_R obtained from the phase shift analysis. The $L_{1/2}$ is the angular momentum corresponding to $|S_L|^2 = 1/2$, and reflected in determining the R_s defined as $R_s = \{\eta + \sqrt{\eta^2 + L_{1/2}(L_{1/2} + 1)}\}/k$. As Table 3 shows, both the $L_{1/2}$ and R_s values increase as the target mass is heavier. The strong absorption radius can further be used to calculate the geometrical reaction cross section σ_{R_s} ($\sigma_{R_s} = \pi R_s^2$), and the predicted σ_{R_s} values are comparable to the ones (σ_R) obtained from partial wave sum.

One of the concerns of this paper is also to obtain the optical potential from the analysis of elastic scattering data. As mentioned in previous section, three-parameter phase shift model provides an analytic expression Eq. (13) of the optical potential from the method of inversion. The solid curves in Figs. 3 and 4 show the real and imaginary parts of the inversion potentials obtained from Eq. (13) using the parameter values determined from TPPSM fit to the elastic data. On the other hand, the dotted curves in these figures denote the Woods-Saxon optical potentials determined from Nadasen *et al.* [12] by fitting the same experimental data. As these figures show, two potentials agree quite well in the surface region around the strong absorption radius. On the contrary, both the real and imaginary parts of inversion potential are found to be different from ones of Woods-Saxon optical potential in the interior region, except for the real potential of ${}^6\text{Li} + {}^{12}\text{C}$ system. Such large differences between solid and dashed curves in the interior region are of little significance because the elastic scattering data are mainly sensitive to the optical potential at surface region.

The form of proposed phase shift Eq. (10) is motivated by the one of Coulomb-modified Glauber model. Thus, it is useful to briefly discuss the physical content from the comparisons of CMGM phase shift with TPPSM phase shift. Using the Eq. (11) one can estimate the NN amplitude parameters (α_{NN} and σ_{NN}) and density parameters from fitting parameters δ_{0R} , δ_{0I} and c given in Table 1. The calculated parameter values are: (1) $\alpha_{NN} = 1.301$, $\sigma_{NN} = 66.58 \text{ mb}$ and $a_P^2 + a_T^2 = 9.653 \text{ fm}^2$ for ${}^6\text{Li} + {}^{12}\text{C}$ scattering, and (2) $\alpha_{NN} = 1.447$, $\sigma_{NN} = 54.49 \text{ mb}$ and $a_P^2 + a_T^2 = 12.361 \text{ fm}^2$ for ${}^6\text{Li} + {}^{28}\text{Si}$ scattering. The calculated NN amplitude and density parameters differ from the CMGM parameters given in Table 1. This differences are considered to be due to the fact that the CMGM calculations did not successfully described the elastic scattering data as shown in Fig. 1. The main reasons of poor fit are thought as follows: (1) The NN total cross section value, taking into account nuclear medium effect [20], is generally decreased. But we used the free space NN total cross section in this study. (2) Since the value of slope parameter β_{NN} at 53 MeV/nucleon is not known, CMGM calculations were done assuming $\beta_{NN} = 0 \text{ fm}^2$.

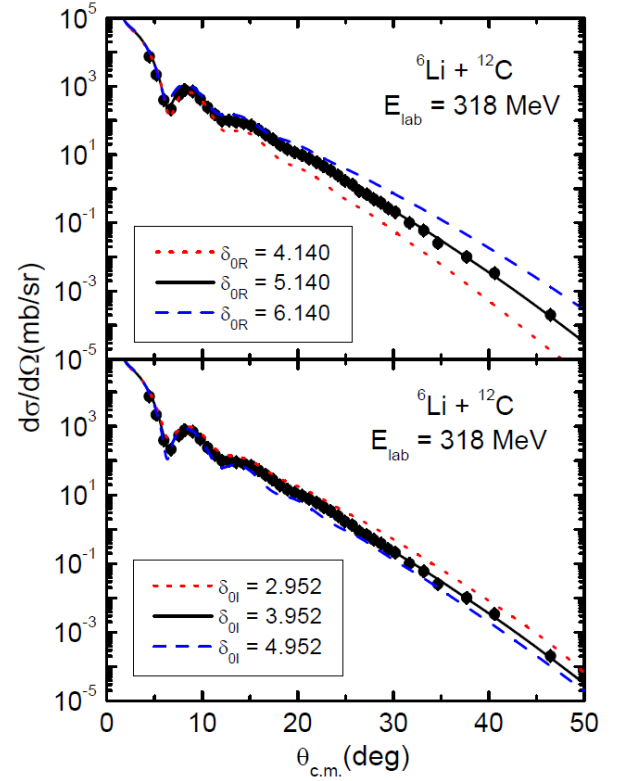


Fig. 5. (Color online) Effect of δ_{0R} and δ_{0I} corresponding to the input parameters of the three-parameter phase shift model on the elastic cross sections of ${}^6\text{Li} + {}^{12}\text{C}$ system at $E_{\text{lab}} = 318 \text{ MeV}$. The other input parameters are fixed and given in Table 1.

In order to investigate the effect of input parameter δ_0 (δ_{0R} and δ_{0I}) given in the suggested phase shift Eq. (10) on the elastic angular distribution, we plotted the ${}^6\text{Li} + {}^{12}\text{C}$ elastic cross section in terms of δ_{0R} (δ_{0I}), where other input parameters are fixed. The δ_{0R} (δ_{0I}) values are taken ± 1.0 from the best fit δ_{0R} (δ_{0I}) value listed in Table 1, and the corresponding results are displayed in Fig. 5. The solid curves of this figure denote the best fits with δ_{0R} (δ_{0I}) = 5.140 (3.952), while the dotted and dashed curves are the results obtained by using δ_{0R} (δ_{0I}) ± 1.0 values. This figure shows variational trends of elastic angular distributions as the δ_{0R} (δ_{0I}) values are varied. The elastic cross sections are moved upward (downward) relative to the best fit as δ_{0R} value increases (decreases). On the contrary, an increase (decrease) in the value of δ_{0I} pushed the calculated cross section curve downward (upward). The differences between three curves are more apparently appeared as the scattering angle increases, though three curves show reasonably agreements at forward angle regions. Calcula-

tions for ${}^6\text{Li} + {}^{28}\text{Si}$ elastic scattering (not shown) gave also similar results.

IV. CONCLUDING REMARKS

In this paper, we have simply presented a three-parameter phase shift model. The form of phase shift is the same as the one of Coulomb-modified Glauber model obtained from Gaussian nuclear densities. It has been applied to ${}^6\text{Li} + {}^{12}\text{C}$ and ${}^6\text{Li} + {}^{28}\text{Si}$ elastic scatterings at $E_{lab} = 318$ MeV. This phase shift model reproduced satisfactorily the structures of the elastic cross sections with a characteristics of both the diffractive oscillation at forward angles and smooth exponential falloff pattern at large angles, and showed good agreements with the experimental data. The three-parameter phase shift model were found to do better in reproducing the elastic scattering data, in comparison with the results from the McIntyre parametrized phase shift model having five adjustable parameters. Through the near-side and far-side decompositions of the elastic cross section for two scattering systems, we have shown that the diffractive oscillatory structures observed at forward angles are due to the strong interference between the near-side and far-side components, and the far-side one provided absolute contribution in determining the smooth exponential falloff behavior of the large-angle cross sections.

Using a three-parameter phase shift model, we have calculated the optical potentials by the method of inversion. Both the real and imaginary parts of inversion potentials for each system generated fairly well agreements in the surface regions around the strong absorption radius but differed greatly in the interior regions, in comparison with the results of optical model analysis. This indicates that the elastic scattering cross section depend sensitively upon the optical potential in the surface regions rather than the interior regions. The effect of input parameter δ_0 ($\delta_{0R} + i\delta_{0I}$) of three-parameter phase shift model on the elastic cross section are investigated. When other input parameters except of the δ_{0R} (δ_{0I}) are fixed, the elastic cross sections are moved upward (downward) as the δ_{0R} (δ_{0I}) value increases.

Finally, three-parameter phase shift model works well and provides reasonable optical potentials for ${}^6\text{Li} + {}^{12}\text{C}$ and ${}^6\text{Li} + {}^{28}\text{Si}$ elastic scatterings at $E_{lab} = 318$ MeV. It is worth noting that this phase shift model is an alternative for describing the heavy-ion elastic scattering.

ACKNOWLEDGEMENTS

This work was supported by the 2018 education, research and student guidance grant funded by Jeju National university.

REFERENCES

- [1] D. M. Brink, *Semi-Classical Methods for Nucleus-Nucleus Scattering* (Cambridge Univ. Press, Cambridge, 1985).
- [2] P. Frobrich and R. Lipperheide, *Theory of Nuclear Reaction* (Oxford Science Publications, 1996).
- [3] J. A. McIntyre, K. H. Wang and L. C. Becker, *Phys. Rev.* **117**, 1337 (1960).
- [4] M. C. Mermaz, B. Bonin, M. Buenerd and J. Y. Hostachy, *Phys. Rev. C* **34**, 1988 (1986).
- [5] S. K. Charagi, S. K. Gupta, M. G. Betigeri, C. V. Fernandes and Kuldeep, *Phys. Rev. C* **48**, 1152 (1993).
- [6] M. H. Cha, *J. Korean Phys. Soc.* **49**, 1389 (2006).
- [7] R. I. Badran, H. Badahdah, M. Arafah and R. Khalidi, *Int. J. Mod. Phys. E* **19**, 2199 (2010).
- [8] V. Franco and A. Tekou, *Phys. Rev. C* **16**, 658 (1977).
- [9] J. Chauvin, D. Lebrun, A. Lounis and M. Buenerd, *Phys. Rev. C* **28**, 1970 (1983).
- [10] A. Vitturi and F. Zardi, *Phys. Rev. C* **36**, 1404 (1987).
- [11] Y. J. Kim and M. H. Cha, *J. Korean Phys. Soc.* **27**, 444 (1994).
- [12] A. Nadasen, T. Stevens, J. Farhat, J. Brusoe and P. Schwandt *et al.*, *Phys. Rev. C* **47**, 674 (1993).
- [13] M. E. Farid and M. A. Hassanain, *Nucl. Phys. A* **678**, 39 (2000).
- [14] Y. J. Kim, *New Phys.: Sae Mulli* **66**, 37 (2016).
- [15] I. Ahmad and M. R. Arafah, *Pramana-J. Phys.* **66**, 495 (2006).
- [16] Y. J. Kim, *New Phys.: Sae Mulli* **64**, 389 (2014).
- [17] S. K. Charagi and S. K. Gupta, *Phys. Rev. C* **41**, 1610 (1990).
- [18] H. M. Fayyad, T. H. Rihan and A. M. Awini, *Phys. Rev. C* **53**, 2334 (1996).
- [19] R. C. Fuller, *Phys. Rev. C* **12**, 1561 (1975).
- [20] C. Xiangzhou, F. Jun, S. Wenqing, M. Yugang and W. Jiansong *et al.*, *Phys. Rev. C* **58**, 572 (1998).